Earthquake Seismology, Exploration Seismology, and Engineering Seismology:
How Sweet It is --- Listening to the Earth

Oz Yilmaz, GeoTomo LLC, Houston, TX, USA, and Anatolian Geophysical, Istanbul, Turkey

Summary

The seismic method has three applications with different requirements for band-width and depth-width:
(1) *Earthquake seismology* with a bandwidth up to 10 Hz and a depth of interest down to 100 km,
(2) *Exploration seismology* with a bandwidth up to 100 Hz and a depth of interest down to 10 km, and
(3) *Engineering seismology* with a bandwidth up to 1000 Hz and a depth of interest down to 1 km.

I shall present a case study for each of the three categories of seismology:
(1) *Earthquake seismology* case study: A seismic microzonation to determine soil amplification and liquefaction probability within a municipal area;
(2) *Engineering seismology* case study: A site characterization survey to determine P- and S-wave velocities, and delineate geometry of layers within the soil column;
(3) *Exploration seismology* case study: A large-offset sesimic survey to image complex structures in thrust belts.

Earthquake Seismology Case Study

The August 1999 earthquake with 7.4 magnitude caused a severe damage within the municipality of Izmit, 170 km east of Istanbul. A survey of the damaged buildings was made by the municipal authorities shortly after the earthquake. The Municipal Government decided to conduct a pilot seismic zonation project to determine whether the cause of the damage was poor construction materials and methods or weak soil conditions. In this project (Yilmaz et al., 2006a), we investigated the soil conditions with two objectives in mind: (1) to estimate the seismic model of the soil column at each district so as to determine the geotechnical earthquake engineering parameters, and (2) to map active faults within the municipal area.

We determined the seismic model of the soil column on a district basis within the Municipality of Izmit. Specifically, we conducted refraction seismic survey at 16 locations and estimated the P- and S-wave velocity-depth profiles down to a depth of 30 m. We then combined the seismic velocities with the geotechnical borehole information about the pedology and lithology of the soil column and determined the geotechnical earnthquake engineering parameters for each district. Specifically, we computed the soil amplification and its effective depth

range, design spectrum periods *TA-TB,* and liquefaction probability and depth range.

By applying a nonlinear traveltime tomography (Zhang and Toksoz, 1998) to the first-arrival times picked from the three shot records, we estimated a near-surface P-wave velocity-depth model along the receiver spread at each of the 16 locations. By applying smoothing during the inversion and lateral averaging after the inversion, we then obtained a P-wave velocity-depth profile representative of each location (Figure 1). Next, we identified the off-end shot record with the most pronounced dispersive surface-wave pattern and performed plane-wave decomposition to transform the data from offset-time to phase-velocity versus frequency domain. A dispersion curve associated with the fundamental mode of Rayleigh-type surface waves was picked in the transform domain based on the maximum-energy criterion and inverted to estimate the S-wave velocity as a function of depth as shown in Figure 1 (Park et al., 1999; Xia et al., 1999). The velocity estimation from surface seismic data represents a lateral average over the receiver spread length in contrast with the velocity estimation from borehole seismic measurements which are influenced by localized lithologic anomalies and borehole conditions.
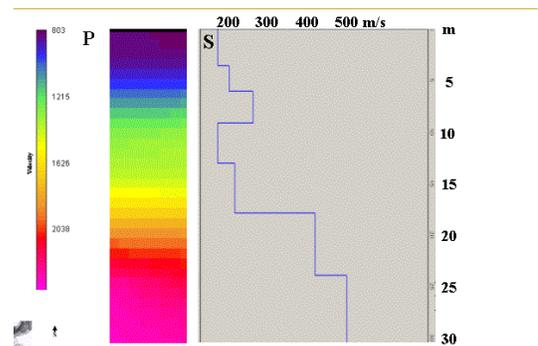

Figure 1. Earthquake seismology case study: The P-wave velocity-depth (left) and the S-wave velocity-depth (right) profiles down to 30-m depth.

To determine the geotechnical earthquake engineering parameter, we began with an SH accelerogram associated with the August 1999 earthquake recorded at a rock site within the municipal area. Given the seismogram at the rock site, we extrapolated it through the soil column knowing the S-wave velocity-depth profile and the geotechnical borehole information to model the

seismogram at the soil site corresponding to the 16 district locations. For each district, we computed the maximum acceleration as a function of depth (Schnabel et al., 1972; Kramer, 1996), and determined the soil amplification factor at the ground level and the depth range for which amplification is significant.

Next, we computed the design spectra --- response of buildings with a range of natural periods to the modeled ground motion at the soil site and the actual ground motion at the rock site (Kramer, 1996). The building structure is defined as a spring system with a single-degree of freedom. From the design spectra, we determined the design spectrum periods *TA* and *TB*.

We extended the relationship between the S-wave velocity and maxium acceleration (Stokoe, 1988) to account for water saturation in the soil column. Provided certain soil conditions are also met, the liquefaction process occurs when the medium becomes fully saturated, in which case the P-wave velocity increases while the S-wave velocity is unchanged (Yilmaz, 2001). By correlating the *Vp/Vs* ratio with the maximum ground acceleration and the S-wave velocity, all as a function of depth, we determined the liquefaction probability or earthquake-induced settlement and its depth range of occurrence at each of the 16 sites. In this analysis, we also took into account the fines content information from the geotechnical borehole data.

The geotechncial earthquake engineering parameters estimated for the districts of the Izmit Municipality indicate that the cause of the severe damage by the August 1999 earthquake is primarily soil amplification in addition to liquefaction at certain localities. In most districts of the municipality, the soil conditions are such that soil remediation would be very costly. Therefore, use of timber and steel, rather than heavy concrete, for construction material would reduce the structural mass of the buildings and provide safer habitation for the municipal residents.

In addition to geotechnical characterization of the soil column at each district, we also conducted shallow reflection seismic surveys at 10 locations within the municipal area along line traverses with an average length of 450 m primarily in the EW direction and derived seismic images down to a depth of 100 m. In contrast with a comprehensive processing sequence applied to reflection seismic data used in exploration for oil and gas fields (Yilmaz, 2001), shallow reflection seismic data usually require a simple processing sequence (Steeples and Miller, 1990) that includes application of a bandpass filter and AGC. Aside from deriving a seismic section that represents the subsurface image down a depth of 100 m, we also estimated the near-surface P-wave velocity-depth

model, again using the nonlinear traveltime tomography, for each of the 10 line traverses.

From the interpretation of the seismic sections, we delineated several faults most of which reach the surface and cause significant lateral velocity variations within the near-surface as verified by the first-arrival tomography solution for P-wave velocity-depth models along the line traverses. The fault patterns observed on the seismic sections are oblique to the North Anatolian right-lateral strike-slip fault system with EW orientation in the area. Such fault patterns, combined with the strike-slip fault system, are often associated with pull-apart tectonism. Therefore, the Izmit area, which is the eastern tip of the Marmara Basin, is a transition zone from the dominant strike-slip regime along the North Anatolian Fault System to the pull-apart tectonic regime of the Marmara Basin.

Engineering Seismology Case Study

We present a unified workflow (Yilmaz et al., 2006b) for analysis of shallow seismic data to estimate a near-surface model defined by layer geometries within the soil column, and the P- and S-wave velocities of the layers themselves.

In the unified workflow for engineering seismology presented here, we make use of all three wave types --- reflected, refracted, and surface waves:
 (1) Apply a simple conventional processing sequence to obtain a CMP stack associated with the reflected waves.
 (2) Perform inversion of traveltimes associated with the refracted waves to estimate a near-surface P-wave velocity-depth model and use it to delineate the geometry of the layers within the soil column and the geometry of the soil-bedrock interface.
 (3) Perform inversion of the Rayleigh waves to derive an S-wave velocity profile in depth.

A site investigation for determination of the seismic parameters of the soil column based on the unified workflow outlined above led to the discovery of a buried lake deposits (Figure 2) near the shores of the Marmara Sea, west of Istanbul.

The shallow reflection seismic data were acquired with common-spread recording geometry using a 48-channel seismic recording system with 10-Hz geophones and an explosive source that uses a pipe-gun placed in a 30-cm hole. Both the receiver and shot station intervals are 2-m. A total of more than 2,000 m reflection profiling was conducted along three line traverses over the survey area (Figure 2).
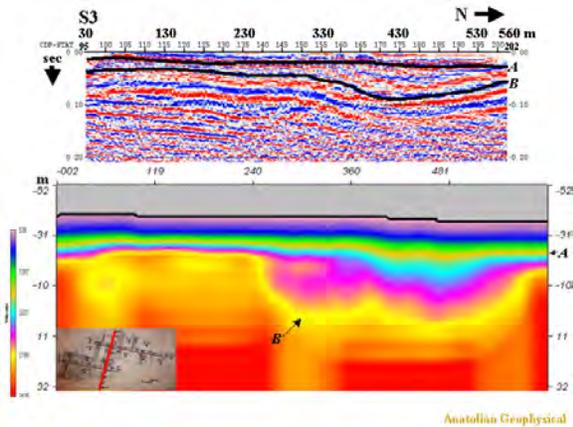
Figure 2. Engineering seismology case study: The seismic section (top) derived from the analysis of reflected waves and the P-wave velocity-depth model (bottom) derived from the analysis of refracted waves. Horizon A defines the boundary between the top soil and the lake deposits, whereas horizon B defines the boundary between the soil-bedrock interface.

Additionally, at 14 locations with 60-m spacing, refraction profiling was conducted using a 48-channel cable with 4.5-Hz geophones at 2-m interval. Shot records were acquired with shot stations at two ends of the receiver cable and at the center of the cable.
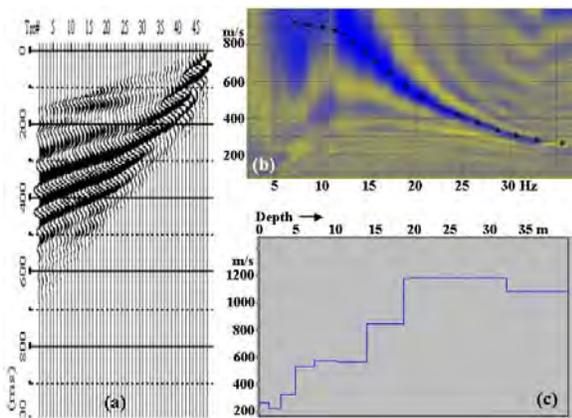
Figure 3. Engineering seismology case study: (a) Surface waves in a field record from a refraction profile (K09) after inside and outside mute to remove refracted and reflected waves; (b) the dispersion curve for the Rayleigh fundamental mode interpreted from the phase velocity spectrum; (c) the S-wave velocity-depth profile estimated from the inversion of the dispersion curve.

While the first breaks from all three shots were used to estimate the P-wave velocity-depth profile at the loaction,

an off-end was used to estimate S-wave velocity-depth proifle from the surface waves (Figure 3). The S-wave velocity-depth profiles were then used to generate depth contour maps for the S-wave velocity field over the survey area (Figure 4). The low-velocity trend coincides with the geometry of the lake deposits.
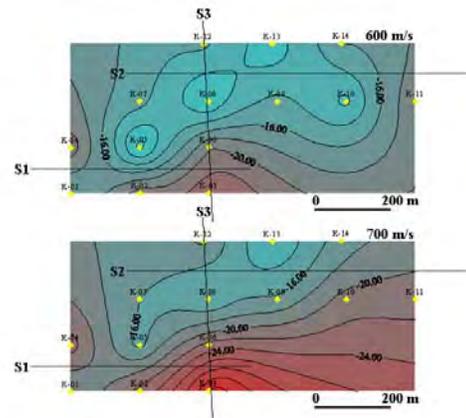

Figure 4. Engineering seismology case study: The S-wave velocity-depth contours over the site. The contours correspond to the maximum depths associated with 600 m/s (top) and 700 m/s (bottom) S-wave velocities.

Exploration Seismology Case Study

Turkish Petroleum Corp. conducted a multichannel large-offset 2-D seismic survey near the town of Ergani, Southeast Turkey, in October, 2004. The objective is to image the complex, imbricate target structures in the Southeast Thrust Belt. The data were acquired using a common-spread recording geometry whereby the receiver spread was fixed for all shots. A total of 960 receiver groups was placed along a 23,975-m line traverse in the NNW-SSE dominant structural dip direction at a 25-m interval. A total of 145 shots was fired at a 250-m interval along the line traverse, beginning at a location outside the spread and 6 km away from the first receiver group in the SSE end of the line. The distance between the first and last shot locations is 35,975 m. Shown in Figure 5 is a portion of one of the large-offset shot gathers from the Ergani Line 201. Note that at small offsets the field record is overwhelmed by Rayleigh waves (ground roll) with backscattering, and essentially is void of reflection energy. When the same field record is examined at far offsets beyond the conventional spread length, note the abundance of supercritical reflections at large offsets. These reflections have been known to early researchers in exploration seismology (Richards, 1960).

Land seismic data acquisition with conventional spread length (3,000 m) and conventional processing in midpoint-

offset coordinates may fail to image complex imbricate structures associated with overthrust tectonics. Irregular topography associated with a rugged terrain, complexity of the near-surface that includes high-velocity layers and outcrops with significant lateral velocity variations, complexity of the overburden caused by allocthonous rocks, and the complexity of the target imbricate structures themselves, all pose challenges to exploration in thrust belts.

We analyzed the Ergani large-offset data for earth modeling and imaging in depth. By a nonlinear first-arrival traveltime tomography, a velocity-depth model was estimated for the near-surface. Then, a subsurface velocity-depth model was estimated based on rms velocities derived from prestack time migration of shot gathers. Finally, prestack depth migration of shot gathers from a floating datum that is a close representation of the topography was performed to generate the subsurface image in depth.
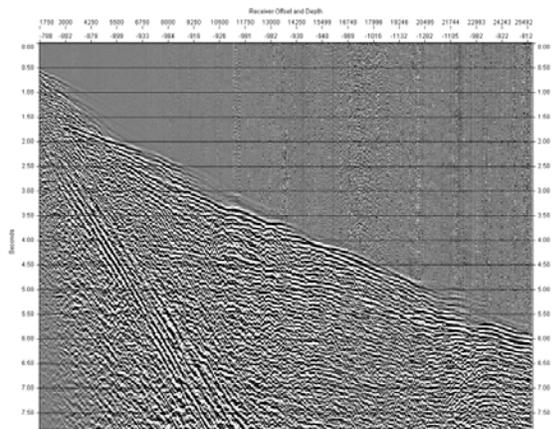

Figure 5. Exploration seismology case study: A portion of a field record from the large-offset Ergani seismic survey with offset range 1,750-25,500 m. Note the abundance of reflections at large offsets and the predominance of the ground-roll energy at near offsets.

Figure 6 shows the image from poststack time migration of the data from Line 221 recorded with conventional spread length (less than 3,000 m) along the same line traverse as that of the large-offset seismic line 201. The data analysis was done using a conventional processing workflow. Note the absence of any coherent signal in this section. It would not matter if the imaging was performed before or after stack, in time or in depth --- the primary cause of this poor image is that the shot records from the vintage line 221 contain weak reflection signal overwhelmed by strong surface waves within the conventional spread length that corresponds to the subcritical region of wave propagation.

In contrast, in prestack migration of the data from Line 201, we made use of the supercritical reflections recorded at large offsets. Another major difference in the data analysis of the two seismic lines is that we migrated the large-offset data from a floating datum, not from a flat datum as in the case of the conventional data. The shot-domain analysis of the data from the large-offset Ergani seismic survey based on common-spread recording geometry has indeed unraveled the imbricate structures that can lead to significant discoveries in the Southeast Thrust Belt.
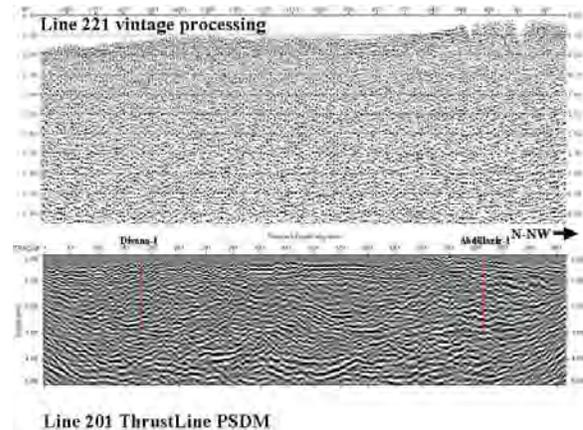

Figure 6. Exploration seismology case study: Top: Poststack time migration of the data from Line 221 recorded with common-midpoint geometry and conventional spread length (less than 3,000 m) along the same line traverse as the large-offset seismic line 201. The data analysis was done using a conventional processing workflow. Bottom: Prestack depth migration of the large-offset data recorded with common-spread geometry. The length of this section spans the full extent of the receiver spread (24 km) down to 5 km. The section is posted with respect to a seismic reference datum of –1,300 m. A 6-30 Hz bandpass filter has been applied to both sections.